

Conductance characteristics between a normal metal and a two-band superconductor carrying a supercurrent

V. Lukic* and E. J. Nicol†

Department of Physics, University of Guelph, Guelph, Ontario, Canada N1G 2W1

(Received 30 April 2007; published 12 October 2007)

The conductance is calculated for a point contact junction between a normal metal and a two-band superconductor with a supercurrent applied parallel to the junction interface. Predictions are made for the case of MgB_2 , which would allow for the determination of the two energy scales and interband coupling. In addition, the generic features of two-band superconductivity in this configuration are studied and contrasted with the one-band case. It is found that two peaks are possible in the zero bias conductance as a function of superfluid momentum q_s for the case of two-band superconductivity, whereas only one could occur in the one-band case. We analyze the case of highly decoupled bands to examine further the potential signatures of interband coupling.

DOI: [10.1103/PhysRevB.76.144508](https://doi.org/10.1103/PhysRevB.76.144508)

PACS number(s): 74.20.-z, 74.50.+r, 74.70.Ad, 74.45.+c

I. INTRODUCTION

A resurgence of interest in two-band superconductivity has occurred with the discovery of superconductivity in MgB_2 .¹ Moreover, possible multiband superconductivity has recently been proposed for a diverse number of materials such as V_3Si ,² Nb_3Sn ,³ NbSe_2 ,⁴ Th-doped Y_2C_3 and La_2C_3 ,⁵ $\text{YNi}_2\text{B}_2\text{C}$,⁶ CeCoIn_5 ,⁷ $\text{Pr}_{1-x}\text{LaCe}_x\text{CuO}_4$,⁸ and Sr_2RuO_4 ,⁹ among others. Historically, the theory of two-band superconductivity was first presented by Suhl *et al.*¹⁰ and Moskalenko¹¹ shortly after the advent of BCS theory. Further developments followed as some of the consequences of the theory were calculated¹² and experiments were interpreted suggesting possible two-band superconductivity in some conventional materials such as Nb.¹³ None of these was confirmed in a substantial way at the time. The first possible evidence of two-band superconductivity came from tunneling experiments on Nb-doped SrTiO_3 by Binnig *et al.*,¹⁴ however, further experimental verification is missing and the evidence presented in that paper for the temperature dependence of the gaps is not rigorously supported by the expectation for two-band s -wave superconductors.^{10,15} Consequently, the discovery of all the hallmarks of two-band superconductivity in experiments on MgB_2 , in excellent agreement with theoretical predictions from two-band s -wave Eliashberg theory with parameters determined from band structure calculations, has given rise to an enormous literature within only a few years. Indeed, experimental and theoretical work on this material points to it being a classic example of two-band superconductivity, making it the textbook example by which all others should be compared.

Given that the theory has been so successful in describing the two-band nature of MgB_2 , it encourages further investigations that would allow for the exploration of physics previously unattainable in one-band materials. Such examples would be the understanding of interband coupling effects due to the electron-phonon interaction or impurity scattering or of interference effects between the bands. Indeed, in this work, we propose an experiment for examining issues associated with interband coupling in two-band superconductors, which would be determined through point contact spectroscopy.

One of the most useful tools for determining order parameter symmetry as well as characterizing the surface properties of materials for the purpose of applications has been point contact spectroscopy (PCS).¹⁶ In this technique, a point contact junction (PCJ) is made by pushing a normal metal tip into the surface of a superconductor. Such PCJs have given clear distinctive evidence for two gaps in MgB_2 ,¹⁷⁻¹⁹ which, in turn, have exhibited both the proper magnitude and temperature dependence in accord with two-band Eliashberg theory with no free parameters.¹⁵ This is seen in the tunneling limit of the contact. However, PCJs provide a much greater wealth of information beyond the magnitude of the energy gap. Indeed, if the contact is not in the tunneling limit with an insulating barrier in between, but is more toward the metal-metal contact limit, then Andreev reflection processes²⁰ can occur and these have been shown to provide a very sensitive probe of a sign change in the order parameter, which gives rise to an Andreev bound state at zero energy.²¹⁻²³ This has been one of the experiments used to determine the presence of a d -wave order parameter symmetry in the high T_c cuprates.²⁴ Thus, PCS can be a very versatile technique in providing a range of information about gap symmetry in addition to exhibiting a proven ability to provide quantitatively accurate measurements in comparison with theory. As a result, theoretical predictions have been provided for superconductor-normal-metal (SN) junctions with regard to the expected signatures associated with the Fulde-Ferrell-Larkin-Ovchinnikov state,^{25,26} fluctuations,²⁷ supercurrents in one-band s -wave and d -wave superconductors,²⁸ and Rashba spin-orbit coupling,²⁹ as some examples.

Here, we wish to investigate further SN PCJs associated with two-band s -wave superconductivity, with materials such as MgB_2 in mind. Indeed, we propose the application of a transverse supercurrent as a technique for resolving information about interband coupling in such materials. The experimental realization of SN point contact measurements with a supercurrent has been presented for the case of $\text{YBa}_2\text{Cu}_3\text{O}_{7-5}$,²⁷ which is a d -wave superconductor, and so we are encouraged that a similar experiment can be mounted with a material such as MgB_2 . We consider the case of a

two-band superconductor with a supercurrent, where the current is capable of suppressing superconductivity in the band with the small gap and allowing access to an intermediate state which contains information about the amount of coupling between the bands.

We begin our presentation by summarizing the theoretical background for the problem in terms of the Bogoliubov–de Gennes equations and then apply the Blonder-Tinkham-Klapwijk (BTK) approximation.^{30–32} In this regard, we discuss issues unique to two bands in the presence of an applied current. The usefulness of the BTK approach is that it is able to capture the range of junction behavior, from tunneling to metal contact, and the simplicity of the final form with attendant fitting parameters is universally popular with the experimental community. The disadvantages of this approach are that there are barrier parameters which are not well characterized and must be fitted via experiment. Note that we will assume throughout the paper that the contact is in the Sharvin limit ensuring the applicability of the BTK approximation.

II. THEORETICAL BACKGROUND

To describe the inhomogeneous problem of a junction between a normal metal and a superconductor, a microscopic approach using the Bogoliubov–de Gennes equations is employed. These equations can be written as³³

$$\begin{pmatrix} \hat{H}_0(\mathbf{r}) & \Delta(\mathbf{r}) \\ \Delta^*(\mathbf{r}) & -\hat{H}_0(\mathbf{r}) \end{pmatrix} \psi(\mathbf{r}) = E\psi(\mathbf{r}), \quad (1)$$

where $\hat{H}_0(\mathbf{r}) = -\hbar^2 \nabla^2 / (2m) + U(\mathbf{r}) - \mu$. Here, μ is the chemical potential, m is the effective mass of the particle on either side ($m = m_S$, $x > 0$ and $m = m_N$, $x < 0$), and we will take $\hbar = 1$. In the case of a junction between a normal metal (N) which is taken to occupy $x < 0$ and a superconductor (SC) for $x > 0$, it is standard in the BTK approximation^{30,31} to take the order parameter $\Delta(\mathbf{r}) = \Delta_0 \Theta(x)$. This neglects the proximity effect in which Cooper pairs “leak” from the SC to the N side causing, in the region about $x = 0$, a suppression of Δ on the SC side and a finite Δ on the N side. BTK also approximates the potential $U(\mathbf{r}) = H\delta(x)$, where H represents the strength of the barrier ($H \rightarrow 0$ for metal contact and $H \rightarrow \infty$ for insulating). Thus, the solution to Eq. (1) simplifies to a one-dimensional quantum mechanical barrier problem, where, for $x < 0$ (N), $\psi(x)$ is a plane wave state containing incident and reflected components and, for $x > 0$ (SC), $\psi(x)$ is written in terms of electron- and holelike quasiparticle amplitudes, u and v , respectively. All the wave functions are modeled by plane waves and, in addition, the momenta are approximated by the momentum at the Fermi level (k_F), which can be different on the two sides. By making these approximations, BTK neglects the terms that contribute to the normalized conductance with accuracy Δ/E_F , where E_F is the Fermi energy on the superconducting side.

In this paper, we work with the BTK equations for s -wave superconductivity, written in the presence of a supercurrent which is parallel to the superconductor–normal-metal bound-

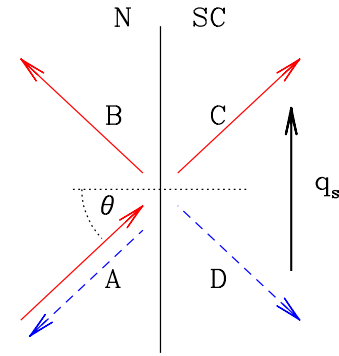


FIG. 1. (Color online) Schematic diagram indicating the geometry of the junction. On the normal metal side, an electron (solid red line) is incident on the boundary at an angle θ and is either specularly reflected as an electron (B) or Andreev reflected as a hole (A, dashed blue line) with an electron (C) and a hole (D) transmitted as quasiparticles on the superconducting side. On the superconducting side, the quasiparticles move in the presence of an applied supercurrent of momentum q_s , which is parallel to the interface.

ary as shown in Fig. 1. We calculate the conductance for each band separately; however, the two-band nature enters through the coupling of the order parameters of each band, which are also a function of a supercurrent momentum. A brief summary of this approach follows below.

We begin by summarizing the result for the one-band case with an applied current. If a supercurrent with momentum q_s is induced on the superconducting side of the junction, then the Hamiltonian of Eq. (1) will be modified for the superconducting side to have, what is called, a Doppler shift of $\hbar q_s k_F / m_S$ added to the kinetic energy term and the order parameter becomes q_s dependent, i.e., $\Delta \rightarrow \Delta(q_s)$. With the contact between the normal metal and the superconductor chosen to be in the y - z plane at $x = 0$, we choose q_s to be in the y direction (see Fig. 1). The direction of the applied supercurrent breaks the symmetry of the tunneling problem with respect to rotations around perpendicular incidence. If the propagation angle of the incoming particle is θ_N , measured on the N side from the direction orthogonal to the interface, then the angle of propagation on the SC side is determined by conservation of the parallel momentum, given as $k_N \sin \theta_N = k_S \sin \theta_S$, where we neglect the effect of q_s in this case as $q_s \ll k_F$. For simplicity, we shall assume that $k_S \approx k_N \approx k_F$ and, therefore, $\theta_N = \theta_S = \theta$. If we consider only two dimensions, the angle between the particle momentum k_S on the SC side and the condensate momentum q_s is simply $\chi = \pi/2 - \theta$. The situation is slightly more complicated in the three-dimensional case. We have to define an additional angle ϕ between the projection of the incident momentum k_N in the yz plane and the y direction. Then, $\cos \chi = \sin \theta \cos \phi$. In this paper, the calculations will be done in two dimensions, close to zero temperature and in the clean limit, in order to bring out the structures in the solutions. The effects of finite temperature, impurity scattering, and three dimensionality would be to broaden the features discussed in our work.

With the geometry shown in Fig. 1, the wave functions on the normal metal side and the superconducting sides can be written as

$$\psi_N(x) = \begin{pmatrix} 1 \\ 0 \end{pmatrix} e^{ik_{N\perp}x} + A \begin{pmatrix} 0 \\ 1 \end{pmatrix} e^{-ik_{N\perp}x} + B \begin{pmatrix} 1 \\ 0 \end{pmatrix} e^{-ik_{N\perp}x}, \quad (2a)$$

$$\psi_S(x) = C \begin{pmatrix} u_+ \\ v_+ \end{pmatrix} e^{ik_{S\perp}x} + D \begin{pmatrix} v_- \\ u_- \end{pmatrix} e^{-ik_{S\perp}x}, \quad (2b)$$

where we have factored out the y and z dependences and absorbed any overall phase into the amplitude coefficients. Here, $k_{N\perp} = k_N \cos \theta \approx k_F \cos \theta$ and $k_{S\perp} = k_S \cos \theta_S \approx k_F \cos \theta$. The coefficient A is the amplitude for Andreev reflection, B is for specular reflection, and D and C are for transmission with and without branch crossing, respectively. Since we work in the BTK limit, all contributions to the conductance of order Δ/E_F are neglected, including the change of the momentum of the Andreev reflected quasiparticle due to the SC condensate momentum (which is of the order of $q_s \approx \Delta/v_F \ll k_F$). Thus, as already indicated, the momentum on either side of the junction is fixed to the Fermi momentum, and motion of the condensate enters only through the definition of electron and hole amplitudes u and v as

$$u_{\pm}^2(E, \theta, q_s) = \frac{1}{2} \left(1 + \frac{\sqrt{(E \pm \tilde{\eta})^2 - \Delta(q_s)^2}}{E \pm \tilde{\eta}} \right), \quad (3a)$$

$$v_{\pm}^2(E, \theta, q_s) = \frac{1}{2} \left(1 - \frac{\sqrt{(E \pm \tilde{\eta})^2 - \Delta(q_s)^2}}{E \pm \tilde{\eta}} \right), \quad (3b)$$

where the plus sign designates propagation of the particle along the initial incident angle θ (measured from perpendicular incidence) and the minus sign takes into account that the direction of propagation of the transmitted holelike particle corresponds to the angle $-\theta$. Here, $\tilde{\eta} = v_F q_s \sin(\theta)$. We take $\Delta(q_s)$ from a self-consistent calculation of the BCS gap equation with an applied supercurrent. (Self-consistency of the spatial solution is neglected as it only gives changes of order of Δ/E_F .³⁴) For zero temperature and simple one-band BCS theory, this is given as³⁵

$$\ln\left(\frac{\Delta}{\Delta_0}\right) = 0 \quad \text{for } v_F q_s < \Delta \quad (4a)$$

$$= -\cosh^{-1}\left(\frac{v_F q_s}{\Delta}\right) + \sqrt{1 - \left(\frac{\Delta}{v_F q_s}\right)^2} \quad \text{for } v_F q_s > \Delta, \quad (4b)$$

where $\Delta \equiv \Delta(q_s)$ and $\Delta_0 \equiv \Delta(q_s=0)$. The form of Δ/Δ_0 versus $q_s v_F/\Delta_0$ is shown in the upper frame of Fig. 2. Note that this result is modified for the two-band case as will be discussed further on.

The BTK quantum mechanical boundary conditions are then applied to match the wave functions given in Eq. (2b):

$$\psi_N(x \rightarrow 0^-) = \psi_S(x \rightarrow 0^+), \quad (5a)$$

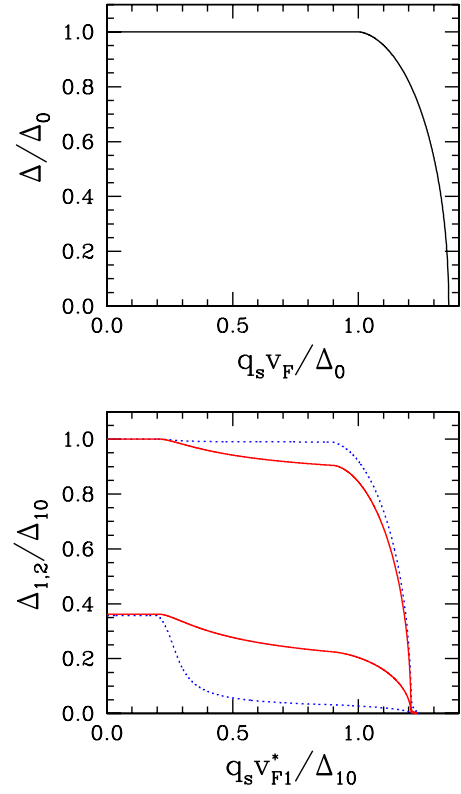


FIG. 2. (Color online) Upper frame: Order parameter Δ/Δ_0 in a one-band s -wave superconductor as a function of $q_s v_F/\Delta_0$. Lower frame: The order parameter for each band (Δ_1 and Δ_2) normalized to $\Delta_{10} = \Delta_1(q_s=0)$ as a function of $q_s v_{F1}^*/\Delta_{10}$ for the case of MgB₂ (solid curves) and that of highly decoupled bands (dotted curves) scaled to match the MgB₂ curves.

$$H\psi_N(x \rightarrow 0^-) = \frac{\hbar^2}{2m_N} \frac{\partial}{\partial x} \psi_N(x \rightarrow 0^-) - \frac{\hbar^2}{2m_S} \frac{\partial}{\partial x} \psi_S(x \rightarrow 0^+). \quad (5b)$$

Also, we define the ratio of Fermi velocities on the two sides as $r = v_F^S/v_F^N$ and $Z = H/\hbar v_F^N$, which measures the delta function barrier strength. In the instance where the barrier strength is renormalized to account for the difference in Fermi velocities, as in Ref. 31, it can be shown that the mismatch of Fermi velocities r and barrier potential H combine into single fitting parameter:

$$\tilde{z}^2 = \frac{Z^2}{r \cos^2 \theta} + \frac{(1-r)^2}{4r}, \quad (6)$$

thus making it a one-parameter theory. This model is strictly one dimensional in nature, i.e., contributions to the overall conductance are calculated separately for each incident angle and summed to obtain the final solution. Finally, we find that the amplitudes of Andreev (A) and specular (B) reflections are

$$A(E, \theta) = \frac{\Delta}{|E + \tilde{\eta}| + (1 + 2\tilde{z}^2)\sqrt{(E + \tilde{\eta})^2 - \Delta^2}}, \quad (7)$$

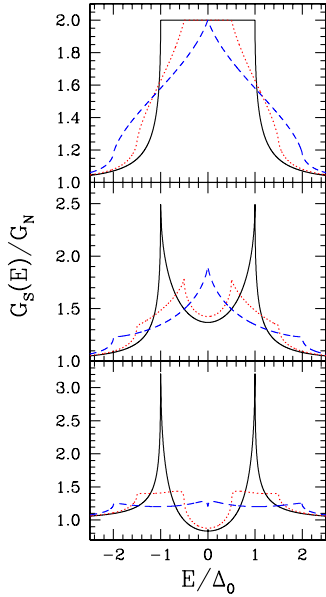


FIG. 3. (Color online) Normalized conductance $G_S(E)/G_N$ at close to zero temperature as a function of E/Δ_0 for a SN PCJ with a one-band superconductor in the presence of a supercurrent. The three frames show results for different Z values ranging from the Andreev limit of $Z=0$ (top frame), $Z=0.25$ (middle frame), and to the near tunneling limit of $Z=0.5$ (bottom frame), with $q_s=0$ (black solid curve), $q_s=0.5\Delta_0/v_F$ (red dotted curve), and $q_s=\Delta_0/v_F$ (blue dashed curve).

$$B(E, \theta) = \frac{2\bar{z}(1 - i\bar{z})\sqrt{(E + \bar{\eta})^2 - \Delta^2}}{|E + \bar{\eta}| + (1 + 2\bar{z}^2)\sqrt{(E + \bar{\eta})^2 - \Delta^2}}, \quad (8)$$

and we find the superconducting state conductance for a single trajectory for one band as $G_S = (1 + |A|^2 - |B|^2)$ and that for the normal state as $G_N = (1 - |B(E = +\infty)|^2)$. G_S has kinks related to the specific Doppler shift energy $\bar{\eta}$. As measured quantities are averaged over all incident angles, we perform an angle average, neglecting the complications due to the details of the Fermi surface (discussed in, for example, Ref. 33): $G_S(E)/G_N = \langle G_S \rangle_\Omega / \langle G_N \rangle_\Omega$. In two dimensions, $\langle \cdots \rangle_\Omega = \frac{1}{\pi} \int_{-\pi/2}^{\pi/2} d\theta$.

In Fig. 3, we reproduce results for a point contact junction between a normal metal and a one-band s -wave superconductor in two dimensions with an applied supercurrent with $v_F^N = v_F^S = v_F$. The results are essentially for zero temperature and are in agreement with similar work of Zhang *et al.*²⁸ shown for higher temperature. For the $q_s=0$ limit (solid black curves), the standard BTK curves are reproduced for the various barrier parameters chosen. With the application of a supercurrent, the curves are modified, and in the case of finite Z , the peaks in the conductance split into two due to the averaged effect of the Doppler shift. Similar results, using a different formalism, have been obtained by Shevchenko.³⁶

To generalize the above one-band approach to the two-band scenario, we take the q_s to be the same in each band and solve for the conductance of each band separately as above; however, for $\Delta(q_s)$, we no longer use the one-band

result of Eq. (4). For a two-band superconductor, the equations for the superconducting order parameter in each band [$\Delta_1 \equiv \Delta_1(q_s)$ and $\Delta_2 \equiv \Delta_2(q_s)$] are coupled and the resulting equation for the two gaps needs to be solved numerically. These equations are based on strong coupling Eliashberg theory and have been reduced in an approximation to a renormalized BCS theory, where they are found to reproduce very well the results of the full theory.^{15,37} We do not reproduce the details here but rather indicate the input parameters and give the final form of the equations which must be solved in order to obtain Δ_1 and Δ_2 as a function of q_s . If Δ_1 is taken to be the larger gap and Δ_2 is the smaller one, then the input parameters are λ_{11} (λ_{22}) for the electron-phonon mass renormalization in the large (small) gap band representing intraband processes, λ_{12} and λ_{21} for scattering between the bands representing interband coupling. Other quantities are the Coulomb pseudopotentials (μ_{11}^* , μ_{22}^* , μ_{12}^* , and μ_{21}^*) and the ratio of the Fermi velocities v_{F2}/v_{F1} . For MgB₂, these parameters have been established from band structure calculations and have been proven to accurately describe a large body of experimental data.¹⁵

At zero temperature, the renormalized two-band BCS gap equations have been evaluated and take the form³⁷

$$\Delta_1 = \bar{\lambda}_{11}\Delta_1\mathcal{G}(\Delta_1, \bar{s}_1) + \bar{\lambda}_{12}\Delta_2\mathcal{G}(\Delta_2, \bar{s}_2), \quad (9a)$$

$$\Delta_2 = \bar{\lambda}_{21}\Delta_1\mathcal{G}(\Delta_1, \bar{s}_1) + \bar{\lambda}_{22}\Delta_2\mathcal{G}(\Delta_2, \bar{s}_2), \quad (9b)$$

where $\lambda_{ij} = (\lambda_{ij} - \mu_{ij}^*)/W_i$, with $W_i = 1 + \lambda_{i1} + \lambda_{i2}$, and

$$\mathcal{G}(\Delta_i, \bar{s}_i) = \ln\left(\frac{2\omega_D}{\Delta_i}\right) \quad \text{for } \bar{s}_i < \Delta_i, \quad (10a)$$

$$= \ln\left(\frac{2\omega_D}{\Delta_i}\right) - \cosh^{-1}\left(\frac{\bar{s}_i}{\Delta_i}\right) + \sqrt{1 - \left(\frac{\Delta_i}{\bar{s}_i}\right)^2} \quad \text{for } \bar{s}_i > \Delta_i, \quad (10b)$$

and $\bar{s}_i = q_s v_{Fi}^* = q_s v_{Fi}/W_i$ and ω_D is a cutoff on the pairing interaction. After solving for the two order parameters for a particular value of q_s the conductance in each band is calculated as in the one-band conductance and these are combined into an overall conductance by introduction of an adjustable parameter, the relative weight α ($0 \leq \alpha \leq 1$), as

$$G(E) = \alpha G(E, \Delta_1, v_{F1}, Z_1) + (1 - \alpha) G(E, \Delta_2, v_{F2}, Z_2). \quad (11)$$

In the lower frame of Fig. 2, we show the solution of Eqs. (9) and (10) for the case of MgB₂, where the parameters are¹⁵ $\lambda_{11} = 1.017$, $\lambda_{22} = 0.448$, $\lambda_{12} = 0.213$, $\lambda_{21} = 0.155$, $\mu_{11}^* = 0.210$, $\mu_{22}^* = 0.172$, $\mu_{12}^* = 0.095$, $\mu_{21}^* = 0.069$, and $v_{F2}/v_{F1} = 1.2$. We also take $v_F^N = v_{F1}$ for all of our two-band calculations. The upper red solid curve is for Δ_1 and the lower red solid curve is for Δ_2 (note that the large gap Δ_1 is associated with the σ band and the small gap Δ_2 with the π band). For the case of MgB₂, there is considerable coupling between the bands, and a consequence of coupling between the bands is that the smaller gap stays finite at the values of $q_s > \Delta_2/v_{F2}$ (a situation that would destroy SC in a one-band case). Simi-

larly, the value of the larger gap is decreased at much smaller values of q_s than in a one-band case. The effect increases with increasing interband coupling, as shown in Fig. 2, where we also give for comparison a highly decoupled case (blue dotted curves). For this latter case, we have used $\lambda_{11}=1.0$, $\lambda_{22}=0.47$, and $\lambda_{12}=\lambda_{21}=0.01$, with $v_{F2}/v_{F1}=1.2$ and $\mu_{ij}^*=0$. These parameters were chosen to produce a relative ratio of the two gaps to match that of MgB_2 , and, for easier comparison with MgB_2 , we have rescaled the x axis so that the curves go to zero at the same point as for MgB_2 .

A very interesting situation arises in MgB_2 . Because of the geometry of Fermi surfaces of this compound, the PCJ conductance is dominated by a π band, the one with the smaller gap, corresponding to values of α between $\alpha=0.25$ for tunneling into the ab plane and $\alpha=0.02$ for a junction along the c axis.¹⁷ In this case, transport would be dominated by the smaller gap band even at values of q_s that would destroy SC in a one-band situation. This would enable us to probe the parameter region which is viewed to be experimentally inaccessible in bulk one-band materials. We note in passing that the region beyond $q_s > \Delta/v_F$ is considered theoretically to be unstable in one-band superconductors,³⁸ however, several experiments found that the region beyond this q_s value was accessible and the result of probing this region was in agreement with the prediction for the evolution of the supercurrent j_s as a function of q_s .^{39–41} While there was debate over this issue in the literature, it was established that the experimental setup probably stabilized the state from the effect of fluctuations.⁴⁰ We would expect this to be the case in two-band superconductors as well, and the situation should be more favorable as coupling to the second band further reduces the region of possible instability.³⁷ It should be noted that it has been proposed theoretically that phase textures may be induced in two-gap superconductors;⁴² however, we ignore this possibility here based on the above arguments. We now continue presenting results for the conductance of two-band superconductors with an applied q_s .

III. RESULTS FOR TWO-BAND CONDUCTANCE

In this section, we illustrate the characteristic results for the conductance of two-band superconductors, comparing the case of MgB_2 (representing high interband coupling) with a case of highly decoupled bands (HDB) for the order parameters shown in the lower frame of Fig. 2.

In Fig. 4, we show results for the MgB_2 case (solid red curves) and the HDB case (dotted blue curves). The frames on the left side show this comparison in the Andreev limit for $Z_1=Z_2=Z=0$ and $q_s/v_{F1}^*\Delta_{10}=0, 0.5, 1.0$ from the top to the bottom frame, while the right hand side displays curves for the same parameters but with $Z=0.5$, which corresponds to being more toward the tunneling limit of the contact. We have taken the relative weighting to be $\alpha=0.25$ for illustration, and the Z 's have been taken to be the same for both bands for simplicity. In the limit of $q_s=0$, the $Z=0$ case gives simply a sum of the two one-band cases and one sees two energy scales referring to the small gap Δ_2 and the large gap Δ_1 . Note, however, that in the $Z=0$ case, the conductance is not constant at a value of 2 throughout low energy region of

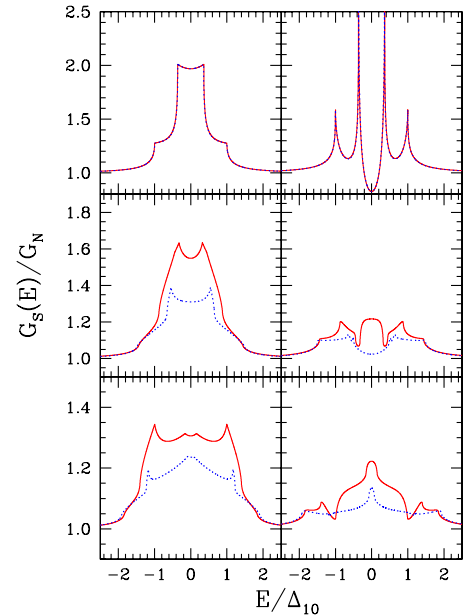


FIG. 4. (Color online) Normalized conductance as a function of E/Δ_{10} for $Z=0$ (three left hand frames), and $Z=0.5$ (three right hand frames) for $v_{F1}^*q_s/\Delta_{10}=0$ (upper frames), 0.5 (middle frames), and 1.0 (bottom frames). Each pair of curves corresponds to MgB_2 (red solid curve) and highly decoupled bands (blue dotted curve).

the curve but rather shows upward curvature, which is a result of the mismatch of the Fermi velocities v_F^N and v_{F2} . As $q_s=0$, there is no difference between the gaps of the MgB_2 and the HDB case, and so the curves sit on top of each other as is illustrated also for the $Z=0.5, q_s=0$ case where one sees the more typical singularities at Δ_1 and Δ_2 associated with regular tunneling. Moving to finite q_s , we now look at the case of $q_s/v_{F1}^*\Delta_{10}=0.5$ in the middle pair of frames. In this region, we have passed the q_s which would have driven the lower band gap to zero, had it been a one-band superconductor. However, due to the coupling with the second band, the Δ_2 is still finite although highly suppressed in the HDB case relative to the case of MgB_2 . Note, however, that the larger gap in MgB_2 is showing more suppression over that of the HDB case. In the conductance curves, we see a clear difference between MgB_2 and the HDB case, especially in the low energy region. In the $Z=0$ case, the peak and inner shoulder features are a result of the Doppler shift due to finite q_s , and with the HDB case, not only is the Δ_2 energy scale shifted, but the overall conductance in the low energy region is reduced. Furthermore, compared to the one-band case for similar Z and q_s , the structure of the curves are quite different from the red dotted curve from the upper frame of Fig. 3. An image of that curve is still seen, but there is substantial modification with an upward curvature at low energies, in particular. The case for $Z=0.5$ (middle right frame) is unlike the curves shown in Fig. 3 (lower frame), and while the decoupled case may be seen to be similar to the dotted red curve of Fig. 3, the MgB_2 case has a hump at zero bias rather than the dip shown in the HDB case. Finally, in the lower frames of Fig. 4, we show the case for $q_s/v_{F1}^*\Delta_{10}=1.0$, where once again the HDB case retains its overall

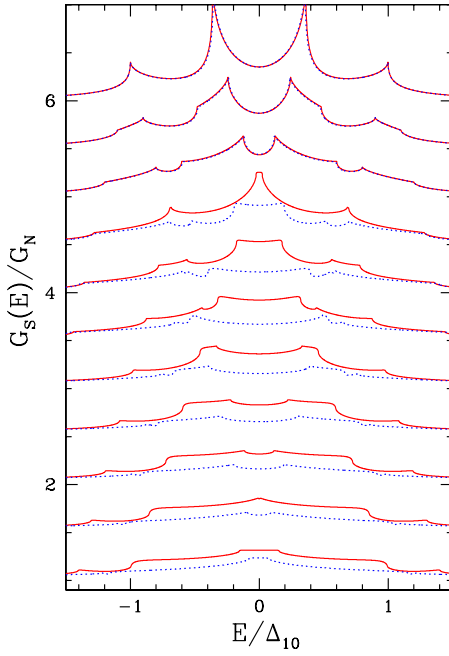


FIG. 5. (Color online) Conductance as a function of E/Δ_{10} for $v_{F1}^*q_s/\Delta_{10}$ varying from 0.0 to 1.0, in steps of 0.1, from top to bottom. Each pair of curves, corresponding to MgB_2 (solid red) and highly decoupled bands (dotted blue) for the same $v_{F1}^*q_s/\Delta_{10}$, is shifted vertically by 0.5 from the previous pair for clarity of presentation

depression relative to the MgB_2 but now the curves for $Z=0.5$ both have a peak at $E=0$ and the MgB_2 curve is particularly uncharacteristic of previously shown curves. The net effect here is a combination of two features. One is the access to q_s values greater than the one-band critical value for the lower gap band and the behavior of the conductance is seen to be different in this region from that of low q_s . The other is due to the Doppler shift which produces additional structures in these curves, which merge with varying q_s . This is more clearly seen in Fig. 5.

In Fig. 5, we plot the conductance for fixed $Z=0.25$ but vary $q_s/v_{F1}^*\Delta_{10}$ in steps of 0.1 (the curves are shown with a successive offset by 0.5 for clarity of presentation).⁴³ Once again, MgB_2 is shown as the solid red curve and the HDB band case is the dotted blue one. Starting with $q_s=0$ for the top curve, one sees two sets of tunneling peaks corresponding to Δ_1 and Δ_2 . As q_s becomes finite, the two peaks split into two in the characteristic manner of the average Doppler shift, producing two edges connected by a curve with downward slope with increasing $|E|$. These shoulders or edges due to the Doppler shift are separated further with increasing q_s , and the inner-moving ones of the Δ_1 band overlap with the outer-moving ones of the Δ_2 band. Whenever two such edges overlap, a peak is found in the conductance and so we see here, over the full range of q_s , that a peak in the conductance at zero bias can occur twice for the two-band case, in contrast with the one-band case where it could occur only once. Indeed, we will discuss this unusual feature further in Figs. 6 and 7.

The difference in conductance of MgB_2 and the HDB case is caused by the different functional dependence of $\Delta_i(q_s)$ in

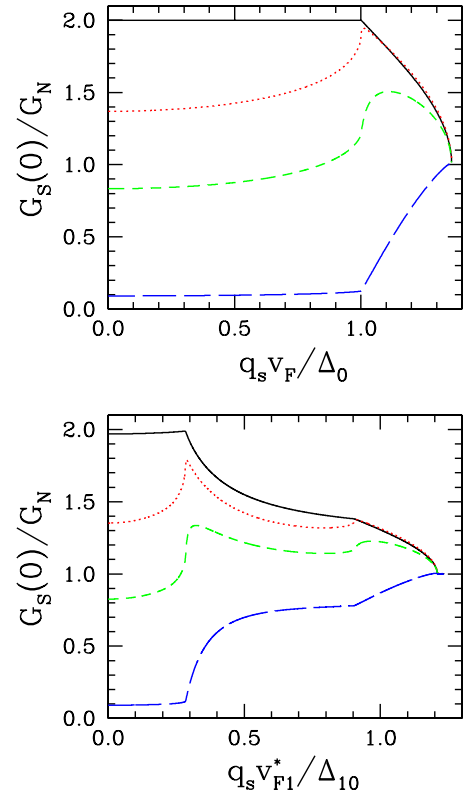


FIG. 6. (Color online) The normalized zero bias conductance $G_S(E=0)/G_N$ versus q_s for the one-band case (upper frame) and MgB_2 (lower frame). Curves are shown for $Z=0$ (black solid), 0.25 (red dotted), 0.5 (green short-dashed), and 2.0 (blue long-dashed).

the two cases. To be specific, let us consider the positions of various peaks in Fig. 5. For a given incident angle, the two peaks at $E=0$ occur as a result of overlap between the two inner peaks of the Δ_2 band when the condensate momentum is given by $\tilde{\eta}_2=\Delta_2(q_s)$, and similarly for Δ_1 band when $\tilde{\eta}_1=\Delta_1(q_s)$. Additional structure occurs with the overlap of the inner peak of the Δ_1 band and the outer peak of Δ_2 band, at

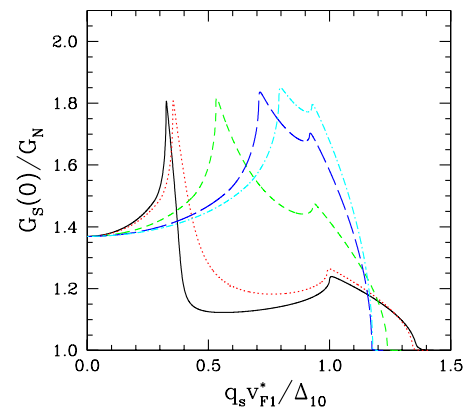


FIG. 7. (Color online) The normalized zero bias conductance $G_S(E=0)/G_N$ versus $q_s v_{F1}^*/\Delta_{10}$ for the two-band case discussed in the text, with varying interband coupling of $\lambda_{12}=\lambda_{21}=0.001$ (solid black), 0.01 (red dotted), 0.1 (green short-dashed), 0.3 (blue long-dashed), and 0.5 (light blue dot-dashed).

energy $E = [\Delta_1(q_s) + \Delta_2(q_s) + \tilde{\eta}_2 - \tilde{\eta}_1]/2$, when the momentum is determined by $\tilde{\eta}_1 + \tilde{\eta}_2 = \Delta_1(q_s) - \Delta_2(q_s)$. Finally, there is an overlap between the inner peak of the Δ_1 band and the inner peak of Δ_2 band originating from a branch with the opposite sign of energy. This occurs at $E = [\Delta_1(q_s) - \Delta_2(q_s) + \tilde{\eta}_2 - \tilde{\eta}_1]/2$, where the momentum is given by $\tilde{\eta}_1 + \tilde{\eta}_2 = \Delta_1(q_s) + \Delta_2(q_s)$.

In Fig. 6, we follow the zero bias conductance (ZBC) as a function of q_s . In the upper frame, we show the result for the one-band s -wave case for four different Z : 0, 0.25, 0.5, and 2.0. For the Andreev limit of $Z=0$, the black solid curve remains at the BTK value of 2 until the value of q_s , where the $\Delta(q_s)$ begins to deviate from 1 and then the ZBC, drops monotonically. For finite Z , the ZBC increases with increasing q_s as the Doppler-shifted peaks from $E = \Delta$ move inward and eventually overlap, producing a peak in the conductance at $q_s = \Delta$ or beyond, although for higher Z values with ZBC below the normal state value, the increase may never show a peak before the order parameter goes to zero at the critical q_c . Another way to understand these peaks is that they are due to the opening of new conductance channels between the upper and lower branches of the superconducting spectrum.⁴⁴

In the lower frame of Fig. 6, we see the case for MgB_2 . In the two-band case, there are two sets of Doppler-shifted peaks, and these peaks will overlap twice at zero energy giving rise to two possible maxima in the ZBC. As in the case of one band, a Z near but not exactly in the Andreev limit is favorable for bringing out these signature structures. Also, note that even for $Z=0$, the ZBC is never 2 as discussed before. While it is clear that in the case of one-band superconductors that one must go near the value of the critical current to see this ZBC maximum, in the two-band case, the first peak can be seen at relatively low q_s relative to the critical value, making it much more likely as a probe of the lower small gap energy scale (where it occurs) and allowing for a measure of interband coupling.

Indeed, in Fig. 7, we show the ZBC for different values of interband coupling indicated in the figure caption using the parameters. $\lambda_{11} = 1.0$, $\lambda_{22} = 0.5$, $\mu_{ij}^* = 0$, $v_{F2}/v_{F1} = 1$, $Z = 0.25$,

and $\alpha = 0.25$. These curves illustrate that with increased interband coupling, not only do the two peaks move closer together due to the gaps moving closer together in energy, but that there is not nearly as dramatic a drop after the first peak, if the coupling is large. Hence, a signature of the interband coupling would be to look at the ZBC in a PCJ, with a contact in the near Andreev limit, and apply a current and vary it to look for the observation of a peak. A study of the position and nature of the peak should provide insight into the magnitude of the interband coupling.

IV. CONCLUSIONS

In summary, we have provided predictions for the conductance of two-band superconductor MgB_2 PCJs in the presence of a supercurrent applied parallel to the interface. Significant differences are seen in the conductance curves relative to the case for one-band superconductors, beyond solely the identification of two energy scales associated with the two energy gaps. Indeed, a study of both MgB_2 and a case of highly decoupled bands, in comparison with the one-band case, reveals peaks in the zero bias conductance at low q_s and unusual structure in $G_S(E)$ versus E , which can be taken as both signatures of two-band superconductivity and provide possible indication of interband coupling. As MgB_2 is well studied and the parameters have been well established, there is expectation that these experiments could be undertaken in that case. Indeed, it may be possible that some variation in the interband coupling has been seen, with a report of weak interband coupling via specific heat in Mg^{10}B_2 ,⁴⁵ which could be further elucidated through study of PCJ conductance.

ACKNOWLEDGMENTS

This work has been supported by NSERC of Canada. We thank J. P. Carbotte, L. Greene, A. J. Leggett, B. G. Nickel, W. K. Park, and J. Wei for interesting and helpful discussions.

*lukic@physics.uoguelph.ca

†nicol@physics.uoguelph.ca

¹J. Nagamatsu, N. Nakagawa, T. Muranaka, Y. Zenitani, and J. Akimitsu, *Nature (London)* **410**, 63 (2001).

²Yu. A. Nefyodov, A. M. Shuvaev, and M. R. Trunin, *Europhys. Lett.* **72**, 638 (2005).

³V. Guritanu, W. Goldacker, F. Bouquet, Y. Wang, R. Lortz, G. Goll, and A. Junod, *Phys. Rev. B* **70**, 184526 (2004).

⁴E. Boaknin, M. A. Tanatar, J. Paglione, D. G. Hawthorn, F. Ronning, R. W. Hill, M. Sutherland, L. Taillefer, J. Sonier, S. M. Hayden, and J. W. Brill, *Phys. Rev. Lett.* **90**, 117003 (2003).

⁵I. A. Sergienko, *Physica B* **359-361**, 581 (2005).

⁶S. Mukhopadhyay, Goutam Sheet, P. Raychaudhuri, and H. Takeya, *Phys. Rev. B* **72**, 014545 (2005).

⁷M. A. Tanatar, Johnpierre Paglione, S. Nakatsui, D. G. Hawthorn, E. Boaknin, R. W. Hill, F. Ronning, M. Sutherland, Louis

Taillefer, C. Petrovic, P. C. Canfield, and Z. Fisk, *Phys. Rev. Lett.* **95**, 067002 (2005); P. M. C. Rourke, M. A. Tanatar, C. S. Turel, J. Berdeklis, J. Y. T. Wei, and C. Petrovic, *ibid.* **94**, 107005 (2005).

⁸Tanmoy Das, R. S. Markiewicz, and A. Bansil, *Phys. Rev. B* **74**, 020506(R) (2006).

⁹A. P. Mackenzie and Y. Maeno, *Rev. Mod. Phys.* **75**, 657 (2003).

¹⁰H. Suhl, B. T. Matthias, and L. R. Walker, *Phys. Rev. Lett.* **3**, 552 (1959).

¹¹V. A. Moskalenko, *Fiz. Met. Metalloved.* **8**, 503 (1959).

¹²For example, T. Soda and Y. Wada, *Prog. Theor. Phys.* **36**, 1111 (1966); C. C. Sung and V. K. Wong, *J. Phys. Chem. Solids* **28**, 1933 (1967); W. S. Chow, *Phys. Rev.* **172**, 467 (1968); R. H. Burkel and W. S. Chow, *Phys. Rev. B* **3**, 779 (1971); V. A. Moshalenko, A. M. Ursu, and N. I. Botoshan, *Phys. Lett.* **44A**, 183 (1973); P. Entel, *Z. Phys. B* **23**, 321 (1976); N. Schophol

- and K. Scharnberg, *Solid State Commun.* **22**, 371 (1977).
- ¹³J. W. Hafstrom, R. M. Rose, and M. L. A. MacVicar, *Phys. Lett.* **30A**, 379 (1969); J. W. Hafstrom and M. L. A. MacVicar, *Phys. Rev. B* **2**, 4511 (1970); J. R. Carlson and C. B. Satterthwaite, *Phys. Rev. Lett.* **24**, 461 (1970).
- ¹⁴G. Binnig, A. Baratoff, H. E. Hoening, and J. G. Bednorz, *Phys. Rev. Lett.* **45**, 1352 (1980).
- ¹⁵E. J. Nicol and J. P. Carbotte, *Phys. Rev. B* **71**, 054501 (2005).
- ¹⁶R. S. Gonnelli, D. Daghero, A. Calzolari, G. A. Ummarino, D. Dellarocca, V. A. Stepanov, S. M. Kazakov, J. Karpinski, C. Portesi, E. Monticone, V. Ferrando, and C. Ferdeghini, *Supercond. Sci. Technol.* **17**, S93 (2004).
- ¹⁷R. S. Gonnelli, D. Daghero, G. A. Ummarino, V. A. Stepanov, J. Jun, S. M. Kazakov, and J. Karpinski, *Phys. Rev. Lett.* **89**, 247004 (2002).
- ¹⁸Y. Boguslavsky, Y. Miyoshi, G. K. Perkins, A. D. Caplin, L. F. Cohen, A. V. Pogrebnyakov, and X. X. Xi, *Phys. Rev. B* **72**, 224506 (2005).
- ¹⁹W. K. Park and L. H. Greene, *Rev. Sci. Instrum.* **77**, 023905 (2006).
- ²⁰A. F. Andreev, *Zh. Eksp. Teor. Fiz.* **46**, 1823 (1964) [*Sov. Phys. JETP* **19**, 1228 (1964)].
- ²¹C.-R. Hu, *Phys. Rev. Lett.* **72**, 1526 (1994).
- ²²Y. Tanaka and S. Kashiwaya, *Phys. Rev. Lett.* **74**, 3451 (1995); S. Kashiwaya, Y. Tanaka, M. Koyanagi, and K. Kajimura, *Phys. Rev. B* **53**, 2667 (1996).
- ²³M. Fogelstrom, D. Rainer, and J. A. Sauls, *Phys. Rev. Lett.* **79**, 281 (1997).
- ²⁴J. Y. T. Wei, N.-C. Yeh, D. F. Garrigus, and M. Strasik, *Phys. Rev. Lett.* **81**, 2542 (1998); H. Aubin, L. H. Greene, S. Jian, and D. G. Hinks, *ibid.* **89**, 177001 (2002).
- ²⁵Q. Cui, C.-R. Hu, J. Y. T. Wei, and K. Yang, *Phys. Rev. B* **73**, 214514 (2006).
- ²⁶Y. Tanaka, Y. Asano, M. Ichioka, and S. Kashiwaya, *Phys. Rev. Lett.* **98**, 077001 (2007).
- ²⁷J. Ngai, P. Morales, and J. Y. T. Wei, *Phys. Rev. B* **72**, 054513 (2005).
- ²⁸D. Zhang, C. S. Ting, and C.-R. Hu, *Phys. Rev. B* **70**, 172508 (2004).
- ²⁹T. Yokoyama, Y. Tanaka, and J. Inoue, arXiv:cond-mat/0605372 (unpublished).
- ³⁰G. E. Blonder, M. Tinkham, and T. M. Klapwijk, *Phys. Rev. B* **25**, 4515 (1982).
- ³¹G. E. Blonder and M. Tinkham, *Phys. Rev. B* **27**, 112 (1983).
- ³²G. E. Blonder, Ph.D. thesis, Harvard University, 1982.
- ³³N. A. Mortensen, K. Flensberg, A.-P. Jauho, *Phys. Rev. B* **59**, 10176 (1999).
- ³⁴V. Lukic, Ph.D. thesis, University of Illinois, Urbana-Champaign, 2005.
- ³⁵K. Maki, in *Superconductivity*, edited by R. D. Parks (Dekker, New York, 1969), p. 1035.
- ³⁶S. N. Shevchenko, *Phys. Rev. B* **74**, 172502 (2006). Also, see references therein for further work in relation to Josephson junctions.
- ³⁷E. J. Nicol and J. P. Carbotte, *Phys. Rev. B* **72**, 014520 (2005).
- ³⁸A. Schmidt, *J. Low Temp. Phys.* **1**, 13 (1969).
- ³⁹A. K. Bhatnagar and E. A. Stern, *Phys. Rev. Lett.* **21**, 1061 (1968).
- ⁴⁰A. K. Bhatnagar and E. A. Stern, *Phys. Rev. B* **8**, 1061 (1973).
- ⁴¹O. P. Hansen, *Phys. Rev.* **181**, 671 (1969).
- ⁴²A. Gurevich and V. M. Vinokur, *Phys. Rev. Lett.* **97**, 137003 (2006).
- ⁴³V. Lukic and E. J. Nicol, *Physica C* **460-462**, 1325 (2007).
- ⁴⁴J. Sanchez-Canizares and F. Sols, *Phys. Rev. B* **55**, 531 (1997).
- ⁴⁵A. Wälte, S.-L. Drechsler, G. Fuchs, K.-H. Müller, K. Nenkov, D. Hinz, and L. Schultz, *Phys. Rev. B* **73**, 064501 (2006).